Quantifying the soil freezing characteristic: the dominant role of salt exclusion

Seth Kwaku Amankwah[1], Andrew Ireson[1], Charles Maule[1], Rosa Brannen[1], and Simon A. Mathias[2]

[1]University of Saskatchewan
[2]Durham University

November 22, 2022

Abstract

The phenomenon of freezing point depression in frozen soils results in the co-existence of ice and liquid water in soil pores at temperatures below 273.15 K, and is thought to have two causes: i) capillary effects, where the phase transition relationship is modified due to soil-air-water-ice interactions, and ii) solute effects, where the presence of salts lowers the freezing temperature. The soil freezing characteristic curve (SFC) characterizes the relationship between liquid water content and temperature in frozen soils. Most hydrological models represent the SFC using only capillary effects with a relationship known as the Generalized Clapeyron Equation (GCE). In this study, we develop and test a salt exclusion model for characterizing the SFC, comparing this with the GCE-based model and a combined capillary-solute effect model. We test these models against measured SFCs in laboratory and field experiments with diverse soil textures and salinities. We consistently found that the GCE-based models under-predicted freezing-point depression. We were able to match the observations with the salt exclusion model and the combined model, suggesting that salinity is a dominant control on the SFC in real soils that always contain solutes. In modelling applications where the salinity is unknown, the soil bulk solute concentration can be treated as a single fitting parameter. Improved characterization of the SFC may result in improvements in coupled mass-heat transport models for simulating hydrological processes in cold regions, particularly the hydraulic properties of frozen soils and the hydraulic head in frozen soils that drives cryosuction.

1   **QUANTIFYING THE SOIL FREEZING CHARACTERISTIC: THE DOMINANT ROLE OF SALT**
2   **EXCLUSION**
3

4   **S. K. Amankwah[1,2], A. M. Ireson[1,2†], C. Maule[2], R. Brannen[2], S.A. Mathias[3]**

5   [1]School of Environment and Sustainability, University of Saskatchewan, Saskatoon, 117 Science
6   place S7N 5C8 Canada.

7   [2]Global Institute for Water Security, University of Saskatchewan, Saskatoon, 11 Innovation
8   Boulevard S7N 3H5 Canada.

9   [3] Department of Engineering, Durham University, Durham, UK.

10

11   Corresponding author: Andrew Ireson (andrew.ireson@usask.ca)

12   † Current Address of corresponding author: Global Institute for Water Security, University of
13   Saskatchewan, Saskatoon, 11 Innovation Boulevard S7N 3H5 Canada

14   **Key Points:**

15   ● Cold regions hydrological models require quantification of the soil freezing characteristic
16   relationship

17   ● The Generalized Clapeyron Equation is found to under predict freezing point depression.

18   ● A salt exclusion model and combined salt-capillary model perform well is simulating
19   observed soil freezing characteristics
20

Abstract

The phenomenon of freezing point depression in frozen soils results in the co-existence of ice and liquid water in soil pores at temperatures below 273.15 K, and is thought to have two causes: i) capillary effects, where the phase transition relationship is modified due to soil-air-water-ice interactions, and ii) solute effects, where the presence of salts lowers the freezing temperature. The soil freezing characteristic curve (SFC) characterizes the relationship between liquid water content and temperature in frozen soils. Most hydrological models represent the SFC using only capillary effects with a relationship known as the Generalized Clapeyron Equation (GCE). In this study, we develop and test a salt exclusion model for characterizing the SFC, comparing this with the GCE-based model and a combined capillary-solute effect model. We test these models against measured SFCs in laboratory and field experiments with diverse soil textures and salinities. We consistently found that the GCE-based models under-predicted freezing-point depression. We were able to match the observations with the salt exclusion model and the combined model, suggesting that salinity is a dominant control on the SFC in real soils that always contain solutes. In modelling applications where the salinity is unknown, the soil bulk solute concentration can be treated as a single fitting parameter. Improved characterization of the SFC may result in improvements in coupled mass-heat transport models for simulating hydrological processes in cold regions, particularly the hydraulic properties of frozen soils and the hydraulic head in frozen soils that drives cryosuction.

Plain Language Summary

When the ground freezes during the winter, not all the water stored in the soil turns into ice, which is because soil particles hold tightly onto some of the water making it impossible to freeze the water and because of the presence of dissolved salts within the soil pore water. The presence of unfrozen water in frozen soils determines the hydraulic properties of the soil which are vital for models of flood forecasting during spring melt, snowmelt infiltration for crop growth and the mechanical properties that determine the stability of the ground for infrastructure in cold regions. In this study, we use laboratory and field experiments, as well as different theoretical models to understand the effect of either or both dissolved salt and soil particles on the amount of unfrozen water stored in the frozen soil, and we suggest that dissolved salts may often be the dominant control. We propose a new relationship for this phenomenon that could improve cold regions hydrological models.

1 Introduction

In cold regions, the way that ice and liquid water are held in the soil pore space plays a significant role in heat, solute and water transport (Spaans & Baker, 1996; He et al., 2016; Watanabe & Osada, 2017), which in turn influence winter evapotranspiration, snowmelt infiltration and runoff (Christensen et al., 2013; He et al., 2016), frost heave formation, thawing settlement, and frost depth penetration in frozen soils (Watanabe & Mizoguchi, 2002; Wen et al., 2012). Good knowledge of the properties of frozen soils is crucial in erosion control and flood risk

56   assessment during spring melt in cold climates. In engineering, information about these properties are employed in

57   infrastructure development such as the construction of roads, pavements, airport runways, bridges and railway lines.

58   Further, in agronomy, these properties are useful in understanding microbial metabolism (Oquist et al., 2009; He et

59   al., 2016; Watanabe & Osada, 2017) and crop water uptake in frozen soils as well as estimating water requirements

60   for winter crops.

61

62   Spontaneous processes, such as the phase change process, occur to minimize free energy. Ice (i) and liquid water (l)

63   can co-exist only when they have equal free energy, and this occurs at 273.15 K (which is defined as T_0) for bulk

64   water (Williams & Smith, 1989, p. 174, Zhang & Liu, 2018), where bulk water is defined as liquid water in an open

65   container that is solute free and at atmospheric pressure. Above T_0, liquid water has lower free energy than ice, and

66   therefore liquid water is the stable phase. When the temperature of pure free water drops below T_0, the free energy

67   of the liquid phase becomes higher than that of the solid phase driving the transformation of liquid water into ice,

68   and ice becomes the stable phase. Unlike bulk water, soil pore water is found to freeze progressively with

69   temperature as the temperature drops below T_0 (Zhang & Liu, 2018; Hayashi, 2013; Williams & Smith, 1989, p.

70   175), a phenomenon termed *freezing point depression*. This was first recognized by Schofield (1935) who used

71   theoretical relationships between sub-zero temperature and matric potential as a means to extend observed soil

72   moisture characteristic curves into drier soil conditions, where tensiometers fail. Early empirical observations of

73   freezing point depression were provided by laboratory experiments reported by Koopmans and Miller (1966) and

74   Williams (1970). Freezing point depression is understood to occur because, in any individual soil pore, the effects of

75   solutes and the attractive forces generated with the soil solids (capillarity and adsorption forces) reduce the free

76   energy of the liquid water, such that the temperature must be less than T_0 for the phase transition to occur. Freezing

77   point depression is therefore attributed to 1) capillarity and adsorption effects (hereafter capillary effects, Williams

78   & Smith, 1989, p. 5; Spaans & Baker, 1996; Zhou et al., 2018), and 2) the presence of salts (Williams & Smith,

79   1989, p 5; Williams, 1970, p. 16; Williams, 1964; Watanabe & Mizoguchi, 2002). The freezing temperature of the

80   depressed liquid water in any individual pore is defined as T_f, (K). Both capillary effects and salt exclusion effects

81   result in progressive freezing, which is to say the water in the continuum of soil pore spaces has a distribution of

82   freezing temperatures and freezing occurs progressively as the temperature drops below T_0. However, the reason

83   these effects are both progressive are different. In terms of capillary effects, the capillary forces and thus the

84   freezing point of the water in an individual pore depends upon the pore size (analogous to matric potential), so

85   smaller pores have lower freezing temperatures (Spaans, 1994). In terms of salts, during freezing, salts are excluded

86   from the ice leaving the remaining solution more concentrated, and thus the freezing temperature of the remaining

87   liquid water is further depressed (Spaans & Baker, 1996; Williams, 1970, p. 17, Banin & Anderson, 1974).

88

89   Freezing point depression is quantified at the soil continuum scale through the soil freezing characteristic curve

90   (SFC). The SFC relates the volumetric liquid water content, θ_l (-), to temperature, T ¿¿C), in frozen soils and is

91   analogous to the soil moisture characteristic curve (SMC), that relates liquid moisture content to matric potential, ψ

92   (m) in unfrozen soils (Spaans & Baker, 1996; Flerchinger et al., 2006; Koopmans & Miller, 1966). The SFC can be

93   directly measured for soils in the laboratory or the field by simultaneous measurements of liquid moisture content

94   and soil temperature. Techniques to measure soil temperature include thermistors (e.g. Spaans & Baker, 1996; Stähli

95   & Stadler, 1997; Bitelli et al., 2003), thermocouples (e.g. Tice et al., 1989; Flerchinger et al., 2006; Watanabe &

96   Wake, 2009; Watanabe et al., 2011) and thermometers (e.g. Watanabe & Mizoguchi, 2002). Techniques employed

97   in measuring the liquid water content include the use of dielectric sensors (Time Domain Reflectometry (TDR),

98   Frequency Domain Reflectometry (FDR), and the Coaxial Impedance Dielectric Reflectometry) (Patterson & Smith,

99   1985; Bitelli et al., 2003; Watanabe et al., 2011; Susha Lekshmi et al., 2014; Zhou et al., 2014; Yao et al., 2016;

100   Tian et al., 2017; Seyfried & Murdock, 2004; Kelleners et al., 2009; Kelleners & Verma, 2010; Kelleners & Norton,

101   2012; Francisca & Montoro, 2012), and the Neutron Magnetic Resonance technique (NMR) (Tice et al., 1982;

102   Yoshikawa & Overduin, 2005; Watanabe & Wake, 2009; Tian et al., 2018). Dielectric sensors are often used to

103   measure water content in unfrozen soils, and work because the dielectric constant of liquid water (~81), is distinct

104   from that of air (~1) and soil solids (4-7) (Susha Lekshmi et al., 2014). The dielectric constant of ice is around 3

105   (West et al., 2007, Kelleners & Norton, 2012), meaning that the bulk dielectric constant of the soil remains

106   dominated by that of the remaining liquid water as the soils freeze, and the ice is essentially invisible to the probe

107   (which can be shown by sensitivity analysis using the dielectric mixing model, presented by Kelleners and Norton,

108   2012). Thus dielectic probes are useful for measuring the liquid water content of frozen soils (useful, for example, to

109   characterize the SFC) but are not useful to measure the total water content (ice plus liquid water, useful, for

110   example, for quantifying the water balance, see Gray and Granger, 1986 who used a two-probe density meter,

111   similar to a neutron probe). Kelleners and Norton (2012) measured SFCs for a range of seasonally frozen soils in

112   Wyoming using the Stevens HydraProbe (Stevens Water monitoring System Inc, 2007). The significant advantage

113   of this instrument is that it simultaneously measures temperature and the bulk dielectric constant – thus directly

114   measuring the SFC. The HydraProbe measures the impedance of a reflected electromagnetic signal propagated

115   through the soil, which is related to the bulk dielectric constant of the soil (Francisca & Montoro, 2012). The

116   measured bulk dielectric constant is then used to estimate the liquid water content through a calibration equation.

117   The HydraProbe measures temperature using a thermistor embedded in the base plate of the sensor head (Seyfried &

118   Murdock, 2004; Kelleners & Norton, 2012). Here, we will use the HydraProbes to measure SFCs in the field and in

119   the laboratory.

120

121   Most models for the SFC that are used in coupled heat and mass transport models for frozen soils (e.g. Hansson et

122   al., 2004, Dall'Amico et al., 2011, Painter & Karra 2014, Clark et al., 2015) are based on predicting the SFC from

123   the SMC using the Generalized Clapeyron Equation (GCE, Williams & Smith, 1989, Kurylyk & Watanabe, 2013).

124   GCE based models assume that in frozen conditions the temperature predicts an equivalent effective soil matric

125   potential, from which the liquid water content can be obtained from the SMC relationship (Zhang & Liu, 2018;

126   Mohammed et al., 2018; Teng, 2020), and hence temperature is related to liquid water content. The advantage of this

127   method is that there are no free parameters associated with the GCE relationship. However, this approach only

128 represents capillary effects (Kurylyk & Watanabe, 2013) and does not account for the effects of solutes on the SFC
129 (Azmatch et al., 2012). Given that real soils do contain solutes this would seem to be a limitation with GCE based
130 models, however, the relative significance of solute effects and capillary effects is not well documented or
131 understood (Watanabe & Mizoguchi, 2002). There are extensive SFC datasets in the literature, from early work by
132 Koopmans and Miller (1966) and Williams (1970) through to recent experimental work by Schafer and Beier
133 (2017), Ren and Vanapalli (2019), Ren and Vanapalli (2020) and Caicedo (2017), and including papers where the
134 solute effects are quantified (e.g. Patterson & Smith, 1985, Zhou et al., 2018). To validate the GCE model requires
135 both observed SFC and SMC data, which are not present in all of these studies. Both Williams (1970) and
136 Koopmans and Miller (1966) present data that shows that for some soils the GCE predicted SFC is consistent with
137 the observed SFC and for others is not, and they suggest that where the GCE fails it may be due to solutes.
138 Koopmans and Miller (1966) found that the GCE works better for finer soils, and suggested that for non-clay soils, a
139 correction factor for the ratio of interfacial tension between water and soils versus water and ice can be applied to
140 improve the predicted SFC. Gharedaghloo et al. (2020) adopted this approach to successfully map the SMC onto the
141 SFC for a series of laboratory experiments, and they used pore scale simulations to demonstrate the differences in
142 ice-entry versus air-entry that this adjustment factor is designed to correct for. In contrast to this, Caicedo (2017)
143 found that the GCE relationship fit SFC observations well for a fine sand and silt soil, while Ren and Vanapalli
144 (2019) found that it did not fit observations well for two different clay soils. Spaans and Baker (1996) used a
145 modified version of the GCE to account for osmotic potential (which the authors conclude is important at
146 temperatures just below 273.15 K) and the temperature dependence of the latent heat of fusion. They suggest that
147 their model matches observations, but they do not present SMC and SFC data independently, meaning that it is not
148 clear how well the standard uncorrected GCE would perform. Schafer and Beier (2017) applied the Spaans and
149 Baker (1996) model to a range of soils with mixed results, and suggest that limitations in performance maybe due to
150 the presence of solutes. Zhou et al. (2018) extended the Generalized Clapeyron Equation to account for solute
151 effects, and showed that their model was able to reproduce SFCs for saline soils from various laboratory
152 experiments that were reported in the Chinese literature. In summary, the performance of the "standard" GCE model
153 is mixed, and the instances where this model fails suggest it may not be a good model to adopt uncritically in
154 coupled heat and mass transport models. Corrections that have been proposed for solutes or for differences in
155 surface tension do not seem to work universally, and hence understandably have not been adopted in coupled
156 models.

157

158 This study was designed to obtain both field and laboratory data that quantifies the SMC and SFC for different soil
159 textures and salinities and to compare the results with those obtained from three different models: 1) capillary effects
160 (the GCE approach); 2) salt exclusion effects; 3) combined capillary and salt exclusion effects.

161 **2 Materials and Methods**

162 **2.1 Laboratory Experiments**

163 The objective of the laboratory experiments was to measure the SMC and SFC of silica sand under controlled

164 conditions. Silica sand was used with de-ionized water to give very low dissolved solutes in the pore water. The

165 silica sand used was a fine-medium standard graded sand (ASTM C778 graded sand from Ottawa, Illinois Region,

166 United States) with particle size ranging from 0.1 mm to 1 mm. The particle size was determined using the

167 mechanical shaking method (Yan et al., 2017; Pekrioglu Balkis, 2019) with a set of sieves. The sand has a measured

168 particle density of 2.5 g cm^{-3}, an estimated bulk density of 1.45 g cm^{-3}, and a porosity of 0.42. The particle density

169 was measured using the pycnometer method as described by Pires et al. (2015), and the soil porosity was determined

170 as the saturated volumetric moisture content of the soil. In both methods, adequate soil packing was achieved by

171 carefully beating the sides of the soil container with a wooden meter rule until there was no change in the level of

172 the sand in the container. If the level of the sand dropped, more sand was added, and the beating repeated. The bulk

173 density of the sand was computed from the measured particle density and porosity.

174

175 The SMC of the sand was measured using the HYPROP set-up (UMS GmBH in Munich, Germany). The sand was

176 repacked into the sampling ring of the HYPROP using the same packing techniques as described in the previous

177 paragraph. Following soil packing, the sample was saturated by placing the sampling ring in a bowl of de-aired

178 distilled water for 24 hours. After 24 hours, the sampling ring was removed from the bowl and placed on top of the

179 sensor unit of the equipment. The soil was then allowed to dry by evaporation. Soil moisture content and matric

180 potential were measured simultaneously by the HYPROP using a mass balance (with an accuracy of ±0.001 g) and

181 two vertically offset tensiometers (has an accuracy of ±0.015 m) (Breitmeyer & Fissel, 2017), respectively. Soil

182 moisture and matric potential measurements were automatically logged at different time intervals.

183

184 The SFC of the same sand was measured using a soil column with dimensions 20 cm (diameter) by 40 cm (height).

185 The column was made from PVC pipe with one end glued on to an acrylic plexiglass using a waterproof JB weld

186 Epoxy. The column was insulated at the side with two layers of single-faced fiberglass to minimize horizontal

187 temperature propagation through the column. The top of the column was left open so that freezing would begin from

188 the surface of the soil. The bottom of the column was not insulated, but the acrylic plexiglass seal at the bottom of

189 the column was thick enough to prevent freezing from beneath the columns. The soil was prepared at two different

190 target moisture contents, 0.05 m^3 m^{-3} and 0.24 m^3 m^{-3} by thoroughly mixing by hand the appropriate amount of oven-

191 dried soil and de-ionized water in a 34 liters (l) plastic container. For the saline treatments, the appropriate mass of

192 salt was weighed and dissolved completely in the appropriate amount of de-ionized water before missing with the

193 soil. Sodium chloride salt (sodium chloride, crystalline from Fisher scientific) was used for this experiment. The

194 total volume of soil (V_t), volume of water (V_w), target volumetric liquid moisture content (θ_l), mass of salt (m_s),

195 bulk salt concentration ($c_b = m_s/V_t$) and pore water salt concentration ($c_s = m_s/V_w$) used for the freezing

196 experiments are detailed in Table 1. The soil was then packed into the columns at 5 cm intervals and compacted with

197   the base of a 250 ml flat bottom flask. Three pre-calibrated Stevens HydraProbes were inserted vertically into the

198   soil at 5 cm, 15 cm, and 30 cm depths in the columns. The Stevens HydraProbe was used because of three reasons 1)

199   it was readily available 2) it can measure soil moisture content and temperature simultaneously and 3) it is the same

200   instrument used in our field experiments. The Stevens HydraProbe measures soil moisture content using the

201   dielectric method, which relates the measured dielectric constant to the moisture content through a calibration

202   equation (calibration equation specified by the Stevens Water monitoring System Inc, 2007). At each soil depth, a

203   probe was inserted vertically into the soil, and the soil was packed around it. The probes were numbered according

204   to their position within the column (probe 1 at 5 cm, probe 2 at 15 cm, and probe 3 at 30 cm, all from the start of the

205   tines of the probes which are about 5.8 cm long). This was to ensure that the same probe was used at the same depth

206   every time the SFC was measured. Following the soil packing, the columns were covered with a polyethylene sheet

207   to prevent evaporation and allowed to sit for two days for moisture to equilibrate in the columns. The columns were

208   then placed in a freezer to measure the SFC. For every treatment, both the freezing and thawing curves were

209   measured. For the freezing runs, the temperature of the freezer was set constantly at 268.15 K. The soil was allowed

210   to freeze until the temperature of all the soil depths approached the freezer temperature or when the moisture content

211   stayed constant. Afterwards, the temperature of the freezer was raised to and kept constant at 277.15 K for the soil to

212   thaw. The thawing runs were terminated when all the soil depths reached a temperature greater than 273.15 K. Soil

213   moisture content ($m^3 \, m^{-3}$) and temperature data (K) were logged every minute using a CR 3000 series data logger

214   from Campbell Scientific.

215

216   **Table 1**

217   *Salt (NaCl) and water treatments used in the laboratory freezing experiment*

Treatment	V_t(l)	θ_l(m³ m⁻³)	V_w(l)	m_S(g)	c_b(g l⁻¹)	c_s(g l⁻¹)
1	12.58	0.05	0.629	0	0	0
2	12.58	0.05	0.629	1.258	0.1	2
3	12.58	0.05	0.629	5.032	0.4	8
4	12.58	0.05	0.629	10.064	0.8	16
5	12.58	0.24	3.0192	0	0	0
6	12.58	0.24	3.0192	6.038	0.48	2

218

2.2 Field Experiments

220   The objective of the field study was to measure the SMC and SFC for different in situ soils with varying texture and

221   salinity. The field studies were conducted at the St Denis National Wildlife Area (SDN) in the Canadian prairies

222   (Bam et al., 2019; Bam & Ireson, 2019) and the Boreal Ecosystem Research and Monitoring Sites (BERMS) Old

223   Jack Pine (OJP) site in the boreal plans ecozone in Saskatchewan (Ireson et al., 2015; Nazarbakhsh et al., 2020).

224

225 The SDN field site is located in the semi-arid, cold Canadian prairies ecozone about 40 km east (106° 5' 36" W, 52°
226 12' 34" N) of Saskatoon, Saskatchewan (Hayashi et al., 1998; Nachshon et al., 2014). The site is partly cropped with
227 wheat, barley, and canola while the rest of the vegetation is a combination of native and introduced grasses (Hayashi
228 et al., 1998, Bam et al., 2019). The site is characterized by an undulating hummocky topography (Hayashi et al.,
229 1998; Nachshon et al., 2014; Bam et al., 2019) with silty stratified sediments and glacial tills (Hayashi et al., 1998;
230 Nachshon et al., 2014; Bam et al., 2019). Soils at SDN can be high in salt, particularly sulphate salts (Nachshon et
231 al., 2014). The site experiences mean annual precipitation (1967-1996) of 358 mm, of which 74 mm occurs as snow
232 (November to April) (Budhathoki, 2018). The mean monthly temperature for the site is 258.45 K for January and
233 February and 291.85 K for July and August (Bam & Ireson, 2019). At SDN, soil moisture data were measured on a
234 transect with three soil profiles, namely upslope, mid-slope and downslope. In this study, however, only observation
235 from the upslope profile is used. Data sets used in the SDN analysis include time series data of soil moisture content
236 (m^3 m^{-3}), soil temperature (K), and matric potential (m) at 5 cm, 20 cm and 50 cm depths. The soil moisture content
237 and soil temperature were measured using Stevens HydraProbes from Campbell Scientific inserted vertically in the
238 soil at the different soil depths. These HydraProbes are the same as those used in the laboratory experiments. The
239 soil matric potential was measured using the 229 heat dissipation matric water potential sensor from Campbell
240 Scientific.
241
242 The OJP site is located east of Prince Albert National Park in the southern Canadian Boreal Forest (104.69° W,
243 53.92° N), Saskatchewan, Canada (Nazarbakhsh et al., 2020). As the name implies, the OJP site is dominated by
244 jack pine (*Pinus banksiana Lamb.)* with an understory of reindeer lichen (*Cladonin spp.*) (Barr et al., 2012;
245 Nazarbakhsh et al., 2020). The soil at OJP is a well-drained sandy soil (Barr et al., 2012; Nazarbakhsh et al., 2020)
246 with a water table depth of at least 5 m below the soil surface (Barr et al., 2012). The OJP site receives an average
247 precipitation of 307 mm (Nazarbakhsh et al., 2020) . It is estimated that about 21 % to 31 % of the total
248 precipitation at this site occurs as snow (Ireson et al., 2015, Nazarbakhsh et al., 2020). The site experiences a mean
249 monthly temperature of around 263.15 K in January and 293.15 K in July (Nazarbakhsh et al., 2020). For the OJP
250 site, soil moisture content and temperature data sets for different soil depths exist. However, in this current study,
251 soil temperature data at 5 cm depth and moisture content data at the top 15 cm were used. The reason is that the soils
252 at the OJP site do not freeze much below 15 cm, which could be because the trees and understory provide insulation
253 that keeps the soil warm. This site also does not have matric potential measurements, which are needed for
254 establishing the SMC. As such, SMC data set published by Cuenca et al. (1997) for the same field site was used in
255 this study. Cuenca et al. (1997) measured moisture content using both the neutron probe (Campbell Pacific Nuclear
256 503 Hydroprobe) and the TDR. Soil matric potential was also measured using a combination of in situ tension disk
257 infiltrometers and water retention data from the laboratory (measured using soil cores). These experiments are
258 described in detail by Cuenca et al. (1997). The raw data points were extracted from the original plot using
259 WebPlotDigitizer (Version 4.2) (Rohatgi, 2015).

260 **2.3 Modeling**

261 As noted earlier, two possible causes of freezing point depression in soils have been identified: i) capillary effects

262 (capillarity and adsorption effects on the free-energy of the pore-water, which is related to the soil pore-size

263 distribution); and ii) solute effects (the effect of dissolved salts on the freezing temperature of free water,

264 independent of the soil pore-size distribution). In this study, models are applied to simulate the soil freezing

265 characteristic curve assuming: 1) capillary effects alone; 2) salt exclusion effects alone; and 3) combined capillary

266 and solute effects.

267

268 Note that here, the unit of temperature is always in Kelvin. The freezing temperature for free pure water at

269 atmospheric pressure is denoted T_0 and has a value of 273.15 K. The freezing temperature of water in a specific part

270 of the soil pore space is denoted T_f. For convenience, we plot SFC curves using the freezing point depression of soil

271 water, denoted T_d and defined as

272

$$T_d = T_f - T_0 \tag{1}$$

273

274

275

276 **2.3.1 Capillary Model**

277 When two phases of a pure substance (e.g. water and ice) are in equilibrium with one another, the temperature and

278 Gibbs free energy (expressed here on a per unit mass basis), G (J kg^{-1}), of each phase must be the same, though the

279 pressures, P (Pa), may differ (for example consider liquid water and water vapour at the water-air interface in a

280 capillary tube). When there is a change in temperature or pressure a new equilibrium state will be reached, again

281 with identical T and G in each phase, such that the change in Gibbs free energy, dG must also be the same for each

282 phase. The change in Gibbs free energy is given by (Williams & Smith, 1989, p. 186 and 190)

283

$$dG = -s\,dT + v\,dP \tag{2}$$

284

285 where s (J K^{-1} kg^{-1}) is entropy and v is specific volume (m^3 kg^{-1}). Hence for ice (subscript i) and liquid water

286 (subscript l) we can write

287

$$v_l d\,P_l - v_i d\,P_i = (s_l - s_i)\,dT \tag{3}$$

288

289 During phase change, the change in entropy is due to the consumption or release of latent heat, so that (Williams &

290 Smith, 1989, p. 190)

$$s_l - s_i = \frac{L}{T} \tag{4}$$

291

292   where L (J kg^{-1}) is the latent heat of fusion. Hence we have

293

$$v_l d\,P_l - v_i d\,P_i = \frac{L}{T} dT \tag{5}$$

294

295   Equation 5 is not controversial in the literature, but different assumptions have been made about how to deal with

296   the ice pressure, P_i (Kurklyk and Watanabe, 2013). Here we will adopt the most common assumption for this

297   (Hayashi, 2013, Williams & Smith, 1989, Hansson et al., 2004, Dall'Amico et al., 2011, Painter and Karra 2014,

298   Clark et al., 2015) which is that there is no change in ice pressure, $d\,P_i = 0$. Noting that the density of water, ρ_l (kg

299   m^{-3}) is equal to $1/v_l$, we have

300

$$\frac{d\,P_l}{dT} = \rho_l \frac{L}{T} \tag{6}$$

301

302   Matric potential, ψ (m), is defined from the relationship $P_l - P_a = \psi \rho_l g$, where g (m s^{-2}) is gravitational

303   acceleration and P_a is atmospheric pressure, which can be treated as constant. Hence we have

304

$$\frac{d\psi}{dT} = \frac{L}{Tg} \tag{7}$$

305

306   Integrating this equation between $\left(T = T_0, \psi = 0\right)$ and $\left(T = T_f, \psi = \psi_f\right)$, we have

307

$$\psi_f = \frac{L}{g} \ln\left(\frac{T_f}{T_0}\right) = \frac{L}{g} \ln\left(\frac{T_0 + T_d}{T_0}\right) \tag{8}$$

308

309   Equation 8 is approximately equal to $\psi_f = L/g\left(T_d/T_0\right)$ (since $\ln\left(1 + x\right) \approx x$, Kurylyk and Watanabe, 2013) i.e. a

310   linear relationship between matric potential and temperature, that predicts a matric potential of -124 m for a

311   temperature of -1 K (Hayashi, 2013). Here we use non-linear form in Equation 8 since it will be important in our

312   combined model below. If the soil is partially saturated at the time of freezing, the unfrozen matric potential, ψ_u

313   (m), will be less than zero. Where ψ_u is the equivalent unfrozen matric potential, and is related to the total water

314   content (ice plus liquid), which is not necessarily constant in frozen soil conditions (total water content changes due

315   to movement of liquid water, which can also refreeze in the soil and hence result in an accumulation of ice that the

316   dielectric probes will not register). Ice will only form in the pore space when $\psi_f < \psi_u$. Hence, we have

317

$$\psi_l = \begin{cases} \psi_u & \psi_f \geq \psi_u \\ \dfrac{L}{g} \ln\left(\dfrac{T_0 + T_d}{T_0}\right) & \psi_f < \psi_u \end{cases} \tag{9}$$

318

319   Where ψ_l predicts the liquid water content, θ_l (m³ m⁻³), given here by the van Genuchten equation (VGN) (van

320   Genuchten, 1980; Kelleners & Norton, 2012).

321

$$\theta_l = \theta_r + \left(\theta_s - \theta_r\right)\left(1 + \left(\alpha\,\psi_l\right)^n\right)^{-m} \tag{10}$$

322

323   where θ_r (m³ m⁻³) is the residual moisture content, and θ_s (m³ m⁻³) is the saturated moisture content or porosity,

324   $\alpha\left(m¿¿-1\right)¿$ is approximately the inverse of the air entry matric potential, n and m are dimensionless empirical

325   shape-defining parameters. Note that the total water content of the soil, θ_t (m³ m⁻³), ignoring changes in density of

326   ice versus water, is given by

327

$$\theta_t = \theta_r + \left(\theta_s - \theta_r\right)\left(1 + \left(\alpha\,\psi_u\right)^n\right)^{-m} \tag{11}$$

328

329   and the ice content, θ_i (m³ m⁻³) is given by

330

$$\theta_i = \theta_t - \theta_l \tag{12}$$

331

332   Such that when $\psi_f \geq \psi_u$ then $\theta_t = \theta_l$ and $\theta_i = 0$.

333

334   Combining Equations 9 and 10 results in an SFC relationship between temperature and liquid water content, and this

335   method describes the GCE model discussed in the introduction.

336   **2.3.2 Salt Exclusion Model**

337   In free-water saline solutions, the freezing temperature is depressed below T_0 due to the presence of solutes. Let T_m

338   (K) represent the temperature below T_0 at which a saline solution of a given concentration will freeze (i.e. T_m is for

339   salt exclusion what is T_d for the capillary model). Table 2 shows observed data from Haghighi et al. (2008) for salt

340   concentration against freezing point depression for sodium chloride salt. Moreover, during freezing, salts are

341 excluded from the ice phase, making the remaining solution more concentrated, leading to a further depression in the

342 freezing point of the remaining liquid water (Banin & Anderson, 1974).

343 **Table 2**

344 *Freezing point depression for an aqueous NaCl solution. Here T_m (K) is the minimum temperature*

345 *below T_0 where only liquid water is present, for a given mass concentration of NaCl.*

Salt mass X (%)	1	5	10	15	18
$T_m(K)$	-0.58	-3.04	-6.79	-11.02	-14.29

346

347 X (%) is the mass fraction of salt in an aqueous solution such that

$$X = \frac{m_s}{m_w} 100 = \frac{c}{\rho_l} 100 \tag{13}$$

348 where m_s(g) and m_w(g) are the mass of salt and water, c(g l^{-1}) is the salt concentration, and the density of liquid

349 water here is expressed in units of g l^{-1} (i.e. ρ_l = 1000 g l^{-1}). c is thus given by $10\,X$. The relationship between

350 freezing point depression and salt concentration from Table 2 is well represented by a 2nd order polynomial function

351 passing through the origin,

$$T_m = p_1 c^2 + p_2 c \tag{14}$$

352 where T_m(K) is the minimum temperature below T_0 where only liquid water is present. p_1 and p_2 are found by

353 fitting Equation 14 to the observed data (Table 2) using linear regression. Following the fitting, the values of p_1 and

354 p_2 were found to be -0.00012544 and -0.05561807, respectively. Solving Equation 14 for c leads to

$$c = \frac{-p_2 - \sqrt{p_2^2 + 4 p_1 T_m}}{2 p_1} \tag{15}$$

355

356 Now, assuming that this relationship can apply to pore water within a soil control volume, V (l) with a fixed mass of

357 salt, m_s, then we have

$$c = \frac{\Box_s}{(\Box_l \Box_r) V} = \frac{c_b}{(\Box_l \Box_r)} \qquad (16)$$

358   where c_b (g l^{-1}) is the bulk solute concentration in the soil, i.e. mass of salt per soil control volume, m_s/V. Note that

359   in Equation 16 we subtract the residual water content from θ_l which is equivalent to assuming that solutes are not

360   freely exchanged between the free pore water and the residual water in the soil. We tested our models with and

361   without this assumption and found that the predicted behavior of the model was more consistent with observed SFCs

362   (which do not, normally, freeze to zero liquid water content) with this assumption. In our salt exclusion model, we

363   assume that all of the pore water remains liquid until the temperature drops to T_m, corresponding to the solute

364   concentration, c using Equation 14. As the temperature drops below T_m, the concentration of salt in liquid water

365   increases according to Equation 15, and we find the liquid water content to sustain this concentration from Equation

366   16. Thus combining Equations 15 and 16 and substituting the maximum possible liquid water content in the soil, θ_m,

367   for θ_l we have

$$\theta_m = \theta_r + \frac{2 c_b p_1}{-p_2 - \sqrt{p_2{}^2 + 4 p_1 T_d}} \qquad (17)$$

368   Equation 17 returns the maximum possible liquid water content for a given bulk solute concentration and soil

369   temperature. The actual liquid water content, then, is given by

$$\theta_l = \begin{cases} \theta_t & \theta_m \geq \theta_t \\ \theta_m & \theta_m < \theta_t \end{cases} \qquad (18)$$

370   Where again θ_t is the total water content corresponding to ψ_u. Equations 17 and 18 thus define an SFC relationship

371   that predicts θ_l based on the total water content (which can be given by Equation 11), soil temperature and the bulk

372   soil solute concentration.

373

374   **2.3.3 Combined Model**

375

376   Models in the literature that combine the effects of solutes and capillary effects on freezing point depression do so

377   by summing the osmotic and capillary potentials (Spaans & Baker 1996; Schafer & Beier 2017; Zhou et al., 2018).

378   We instead assume here that the solute depression effect acts to lower the temperature at which freezing is initiated

379   in the absence of capillary effects. Equation 7 (the GCE equation) is therefore integrated between the new limits

380    $(T = T_m, \psi = 0)$ and $(T = T_f, \psi = \psi_f)$, thus giving

381

$$\psi_f = \frac{L}{g} \ln\left(\frac{T_f}{T_m}\right) = \frac{L}{g} \ln\left(\frac{T_0 + T_d}{T_m}\right)$$ (19)

382

383   The challenge we now face is that we have a circular problem: θ_l depends on ψ_f (Equation 10) which depends on

384   T_m (Equation 19) which depends on c (Equation 14) which depends on θ_l (Equation 16). We therefore solve this

385   problem using an iterative approach, as follows: for a given ψ_u, T and c_b we first guess the liquid water content θ_{l0};

386   next we use Equations 10, 19, 14 and 16 in sequence to calculate a new liquid water content, θ_{l1}; next we check the

387   squared error $\left(\theta_{l0} - \theta_{l1}\right)^2$ against some tolerance value (10^{-8}) and if the error is too large we reset our initial guess to

388    $\theta_{l0} = \omega \theta_{l1} + (1 - \omega)\theta_{L0}$ and repeat these steps until convergence. Here ω is a relaxation factor (0-1) that is

389   adjusted to improve the speed of convergence. Using this approach we were able to obtain stable convergence with

390    $\omega = 0.05$. It is possible that an improved mathematical solution procedure could be obtained for this problem, but

391   for our purposes, this approach is adequate.

392

393   **2.3.4 Behaviour of the alternative models**

394
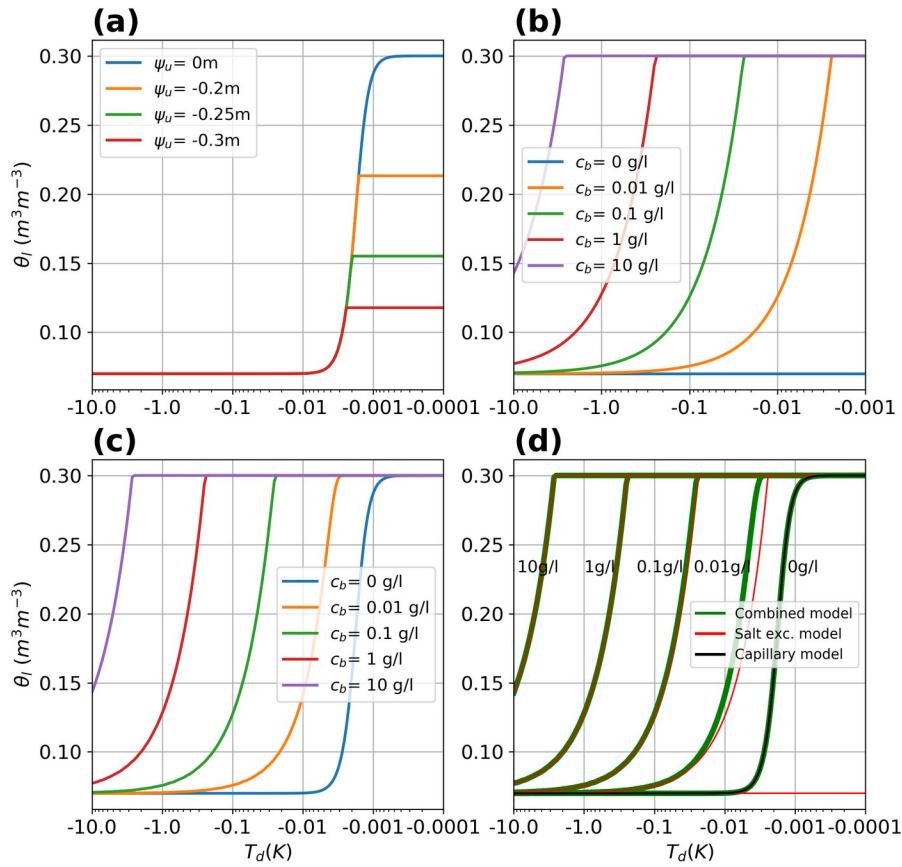
Figure 1. (a) Capillary model simulations with arbitrary soil parameters and differing ψ_u (or differing total water contents), (b) simulated results for the salt exclusion model using arbitrary parameters and differing salt mass (per bulk soil volume), (c) simulations for the combined capillary salt model (Equation 3.14) using arbitrary soil parameter and differing salt mass (per bulk soil volume), and (d) comparing the outcomes of the 3 models.

399

400   **Table 3**

401   *Arbitrary soil parameters used in the model simulations*

402

VGN parameters	Value
α (m^{-1})	-4.79
n	5
m	0.8
θ_{rv} (m^3 m^{-3})	0.07
θ_s (m^3 m^{-3})	0.3

403

404   The three models described above were run using arbitrary soil parameters (Table 3) to produce SFCs plotted in

405   Figure 1. The capillary effect model (Figure 1a) describes the SFC for soils with no solute effects, and was run with

406   different total water contents (represented using different equivalent unfrozen matric potentials ψ_u of 0 m, -0.2 m,

407   -0.25 m and -0.3 m). The soil water remains liquid with reducing soil temperature until it reaches a certain

408   depressed temperature when freezing commences, shown by the decrease in liquid water content with temperature.

409   The salt exclusion model and combined model were both run for saturated conditions with changing bulk solute

410   concentrations (c_b = 0 g l^{-1}, 0.01 g l^{-1}, 0.1 g l^{-1}, 1 g l^{-1}, and 10 g l^{-1}). The simulation results shows that the salt

411   exclusion model (Figure 1b) predicts enhanced freezing point depression with increasing salt concentrations, or in

412   other words, more liquid water remains at the same temperature for higher salt concentrations (represented by a shift

413   of the curve to the left-hand side of the plot). This model simulates no freezing point depression if the solute

414   concentration is zero – a condition that does not occur in real soils. The combined model (Figure 1c) behaves the

415   same as the salt exclusion model at high solute concentrations, and the same as the capillary model with zero solute

416   concentration, as would be expected. For the arbitrary soil that these simulations were run for, the salt exclusion

417   model and combined model only differed noticeably when the solute concentration was less than 0.1 g l^{-1} (Figure

418   1d).

419

420 **3 Results and Discussion**

421 **3.1 Laboratory Experiments**

422   The observed SMC for the silica sand that was measured in a laboratory drying experiment, as described in section

423   2.1, is shown in Figure 2. The van Genuchten model (VGN) was fit to these data. The observed data did not extend

424   up to saturation (i.e. $\psi_u = 0$) which is probably because the soil was not completely saturated at the start of the

425   experiment. The saturated moisture content (θ_s) was set to be equal to the measured porosity of the soil (0.42 m^3 m$^-$

426   ^{3}) The residual moisture content (θ_r) was identified visually from Figure 2. The parameters $n, m,$ and α (Table 4)

427   were obtained by optimization, minimizing the root mean squared error (RMSE) in water content. After fitting the

428   RMSE was 0.017. The green dots are observed data points from the start of the experiment and were excluded from

429   the fitting because they were not consistent with a typical SMC curve. This was likely due to non-equilibrium

430   conditions in the soil sample at the beginning of the experiment. Judging from the results (Figure 2), this soil has

431   poor water retention, and drains rapidly as the matric potential drops below about -0.1 m. The soil reaches its

432   residual moisture content (about 0.02 m^3 m^{-3}) at a matric potential of about -0.38 m. This result is typical of coarse

433   textured soils that lose moisture rapidly due to their large pore sizes.

434

435   SFCs measured in the laboratory for the same sand and with varying pore-water dissolved salt (NaCl) concentrations

436   are plotted in Figure 3 (at a target moisture content of 0.05 m^3 m^{-3}) and Figure 4 (at a target moisture content of 0.24

437   m^3 m^{-3}). The results show, as expected, that higher salinity results in enhanced freezing point depression (curves

438   shift to the left), or in other words, for the same temperature more liquid water is retained in the soil at higher salt

439   concentrations. The results also reveal the phenomenon of supercooling during freezing (depicted by the red-colored

440   ring in the third plot on the third row of Figure 3a). The temperature of the soil decreased to what is termed as the

441   temperature of spontaneous nucleation (T_{SN} ¿(Kozlowski, 2009; Zhou et al., 2020) without a change in moisture

442   content. Supercooling is a metastable stage in freezing and is common in laboratory experiments. T_{SN} is the

443   temperature at which a stable ice nucleus for ice crystallization forms in a freezing soil (Kozlowski, 2009). After

444   reaching the T_{SN} there is a release of latent heat that warms the soil to its freezing point where freezing begins

445   (Kozlowski, 2009; Ren & Vanapalli, 2020; Zhou et al., 2020). The supercooling effect is absent in the thawing

446   curves (Figure 3b and 4b), which is as expected. Depicted in the purple ring (first plot on the first row of Figure 4a)

447   is possible evidence of moisture migration during soil freezing. Here the liquid moisture increased with decreasing

448   soil temperature. This observation may be due to the migration of moisture from unfrozen layers toward the freezing

449   front, a phenomenon termed cryosuction. Experiments of Mizoguchi (1990), as described in Hansson et al. (2004)

450   revealed the same phenomena during soil freezing. According to Hansson et al. (2004), this is due to the high

451   hydraulic gradient established in the soil during freezing which causes moisture to move upwards toward the

452   freezing front.
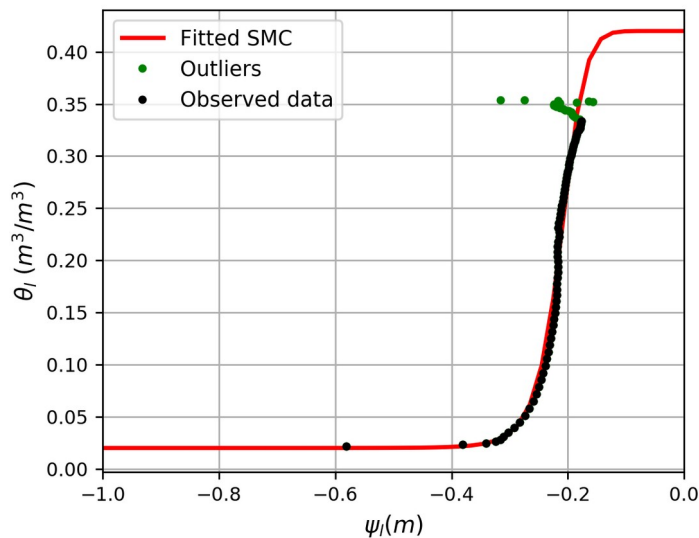
453

454   **Figure 2**. The soil moisture characteristic curve of silica sand measured using the HYPROP apparatus (black dots)

455   and fitted to the van Genuchten model (solid red line)
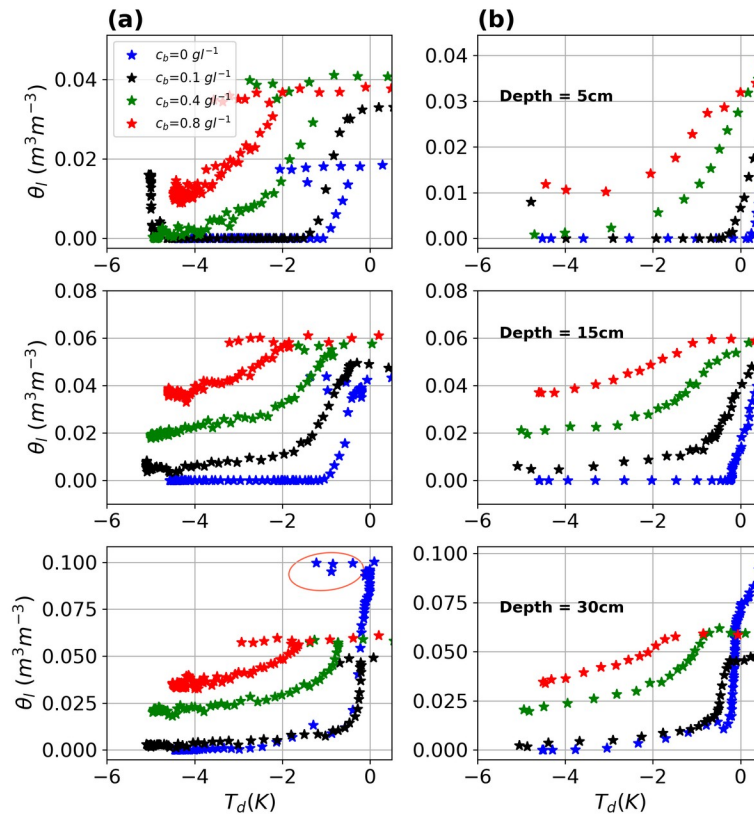
456

457 **Figure 3**. SFCs of the silica sand at different salt concentrations at a target moisture content of 0.05 m³ m⁻³ (a)

458 freezing curves for different soil depth, and (b) thawing curves for different soil depth
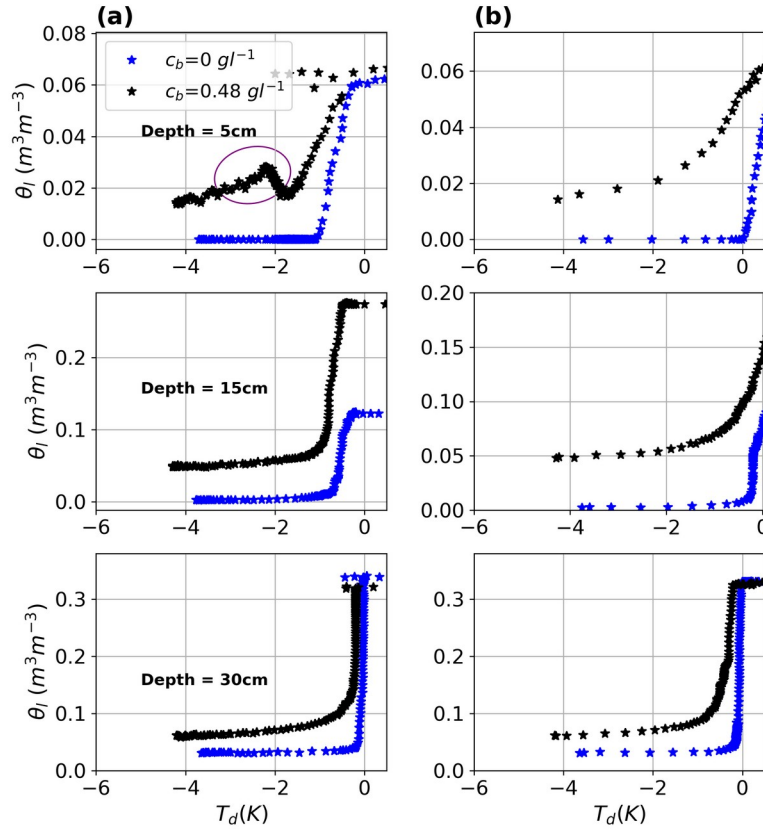
**Figure 4**. SFCs of the silica sand at different salt concentrations at a target moisture content of 0.24 m³ m⁻³ (a) freezing curves for different soil depth, and (b) thawing curves for different soil depth

Table 4

Fitted parameters and RMSE for the SMC of the silica sand

VGN parameters	Value
α (m⁻¹)	-4.79
n	10.11
m	0.90
θ_{rv} (m³ m⁻³)	0.02
θ_s (m³ m⁻³)	0.42

469

3.2 Field experiment

471   Figure 5 is the results for the SDN site: SMCs fitted to the VGN model (solid pink line) (Figure 5a), freezing curves

472   (Figure 5b) and thawing curves (Figure 5c). The results show that the SMCs for the different years are different.

473   Some specific reasons for this observation may include 1) shrinking or swelling of the soils, particularly because the

474   soil here is rich in clay, and 2) the shifting of measuring instruments. The 2013 curves are used in all analysis, since

475   the 2013 curves are wetter than the other years and looks reasonably consistent at all the soil depths. The curves

476   were fitted to the VGN model by minimizing the root mean square error (RMSE), which is calculated from the

477   difference between the observed moisture content and the predicted moisture content from the VGN model (fitting

478   parameters values are documented in Table 5). The results also shows that the total water content at the onset of

479   freezing (Figure 5b) was significantly lower than the total water content at the end of the thawing (Figure 5c). The

480   pre-freeze up water content depends on how much rainfall fell in the late summer or fall months. The post thaw

481   water content depends on moisture migration to the frozen soil over the winter months (cryosuction, which we

482   cannot directly observe, since this water would refreeze and as ice it would be invisible to the dielectric probes), and

483   infiltration of snowmelt that occurs before the soil thaws. The SMC of the OJP site and the VGN model (red line) is

484   shown in Figure 6a (find parameter values in Table 6). Similar to the laboratory soil, the OJP soil is coarse-textured

485   and loses moisture rapidly. Again, we see here that the thawing curve (Figure 6c) ends up wetter than the freezing

486   curves (Figure 6b), which we attribute solely to snowmelt infiltration. The OJP site has very low moisture content;

487   hence moisture migration may not be practical.

488

489

490
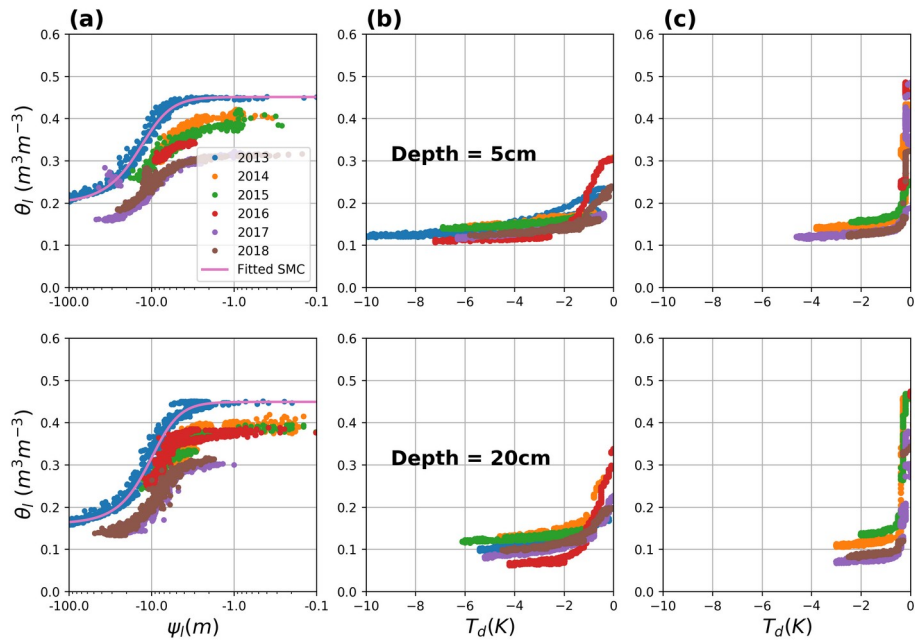
491

492   **Figure 5**. Results for the SDN field site; (a) SMCs for different years fitted to the van Genuchten model (solid

493   purple line), (b) freezing curves for different years, and (c) thawing curves for different years.

494
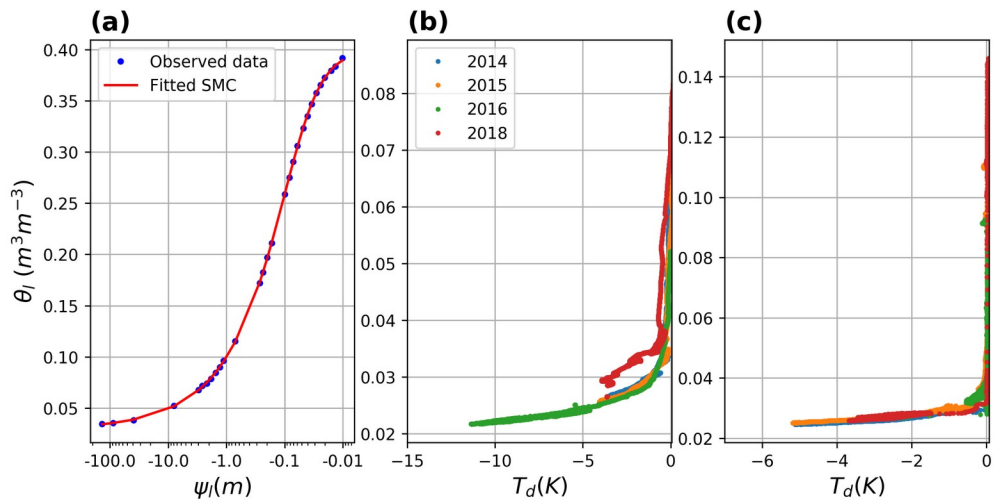
495

496   **Figure 6**. Results for the OJP field site; (a) SMC fitted to the van Genuchten model (solid red line), (b) freezing

497   curves for different years for the top 15 cm depth, and (c) thawing curves for different years for the top 15 cm depth.

498

499

500

501

502

503 **Table 5**

504 *Fitted parameter values of VGN for SDN site*

505

Soil depth	Year	α (m^{-1})	n	m	θ_r (m^3 m^{-3})	θ_s (m^3 m^{-3})	RMSE
5 cm	2013	0.094	2.55	0.61	0.198	0.45	0.0095
20 cm	2013	0.12	2.72	0.63	0.16	0.45	0.0119
50 cm	2013	0.094	2.55	0.61	0.198	0.45	0.0095

506

507

508 **Table 6**

509 *Fitted parameter values of VGN for OJP site*

510

Parameter	α (m^{-1})	n	m	θ_r (m^3 m^{-3})	θ_s (m^3 m^{-3})	RMSE
value	19.44	1.6	0.4	0.03	0.4	0.00076

511

3.3 Model performance

513 Models were run for each of the laboratory and field experiments, to reproduce the SFCs. We found that in many

514 cases, the residual water content, θ_r, was lower for the freezing curves (SFCs) compared with the drying curves

515 (SMCs). This could be an artifact of the probe, but we suspect that this could be a real phenomenon. This suggests

516 that the minimum pore size for drying is larger than the minimum pore size for freezing. Because of this, we

517 adjusted θ_r for our models to match the SFC data.

518

519 The validation results for the three models (capillary, salt exclusion and the combined model) using laboratory

520 measured SFCs are presented in Figure 7 and Figure 8. Here the models were compared with observations from 30

521 cm depth because the shallower probes (5 cm and 15 cm depths) froze rapidly and were possibly not in

522 thermodynamic equilibrium, and hence may overpredict the freezing point depression in the soil. The bulk soil salt

523 concentrations were assumed to remain constant for the duration of the experiment, i.e. we ignore any potential salt

524 redistribution in the soil profile.

525

526 Figure 7 presents the results for the case where no salt was added to the soil in the experiment. In Figure 7a, a value

527 of $c_b = 0$ is used in the salt exclusion and combined models, and the performance of the three models are compared.

528 As expected, the capillary and combined models are identical and the salt exclusion model predicts no freezing point

529 depression. The performance of the capillary model is poor, which suggests that the assumptions within the GCE are

530   inappropriate for this soil. Despite our efforts to minimize solutes (using de-ionized water and pure silica sand), the

531   soil pore water may still contain some amounts of dissolved salts, that may result in higher depression of the

532   freezing point in the SFCs. This was tested by mixing 100 g of sand with 100 ml of deionized water and measuring

533   the electric conductivity (EC) after the mixture was stirred for about 5 minutes and allowed to settle. A calibrated

534   conductivity meter gave a reading of 19 μS cm^{-1}, equivalent to $c_b = 0.024$ g l^{-1} (the EC was converted to c_s, i.e.

535   TDS, by multiplying by 0.64, Chang et al., 1983). Note that this is just an estimate of the salt concentration in the

536   sand since the actual conversion of EC to TDS depends on the activity of the different ions in the sand. When this

537   concentration was used in the combined and salt exclusion models their performance was markedly improved,

538   Figure 7b, though the model still did not fit the observations. These models could be made to fit the observations

539   well by using a value of $c_b = 0.12$g l^{-1}, Figure 7c, determined by manual calibration. This is likely an unrealistically

540   high solute concentration for this experiment. It must be noted that the temperature in Figure 7 is on a log-scale, and

541   the errors in Figure 7a and b are smaller than the reported error tolerance of the temperature observations with the

542   probe ($\pm$ 0.3 K).

543

544   The results for the experiments where a fixed mass of NaCl salt was added to the soil are shown in Figure 8. The

545   poor performance of the capillary model was unchanged, but both the salt exclusion and the combined model

546   performed well without calibration or refinement. Since the predictions from the combined and salt exclusion

547   models were identical, this implies that the SFCs here are completely dominated by the salt exclusion effect.

548
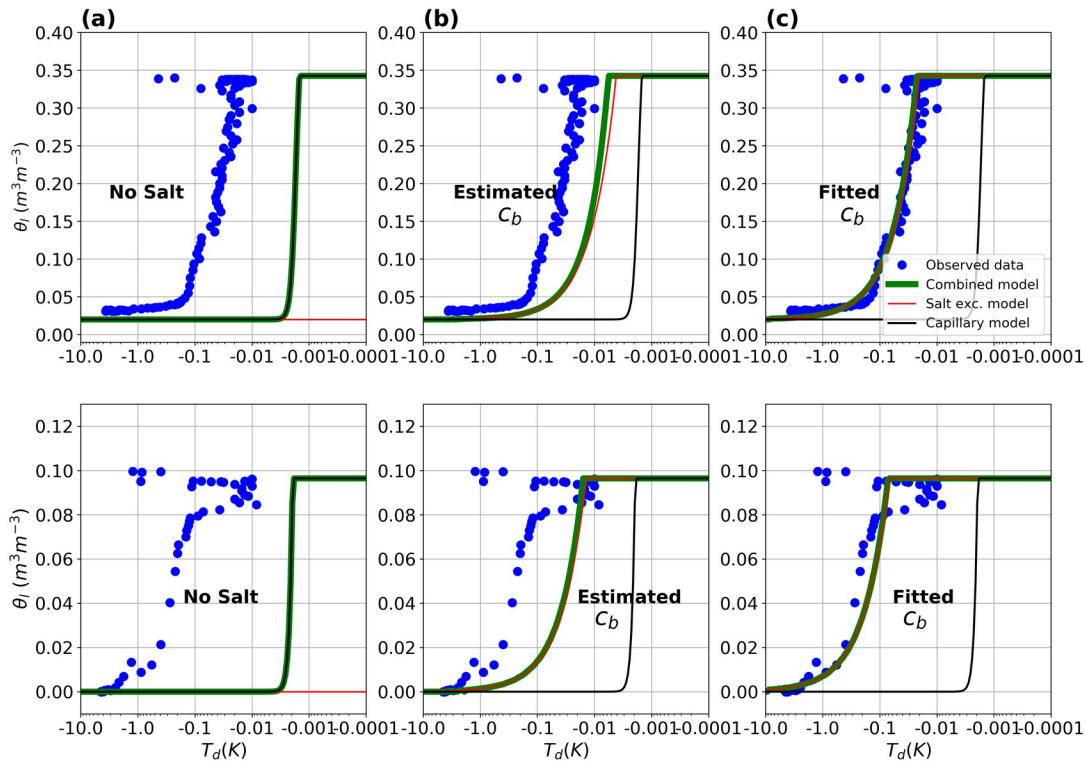
549

550 **Figure 7**. Performance of the three models (capillary, salt-exclusion and combined model) against laboratory

551 observed SFCs at 30 cm depth with no salt added: (a) salt exclusion and combined models with no fitting, $c_b = 0$ g l⁻

552 ¹; (b) salt exclusion and combined models with estimated $c_b = 0.024$ g l⁻¹ and (c) salt exclusion and combined

553 models fitted to the data with $c_b = 0.12$ g l⁻¹. Upper panel is results for higher antecedent moisture content and lower

554 panel is results for lower antecedent moisture content.
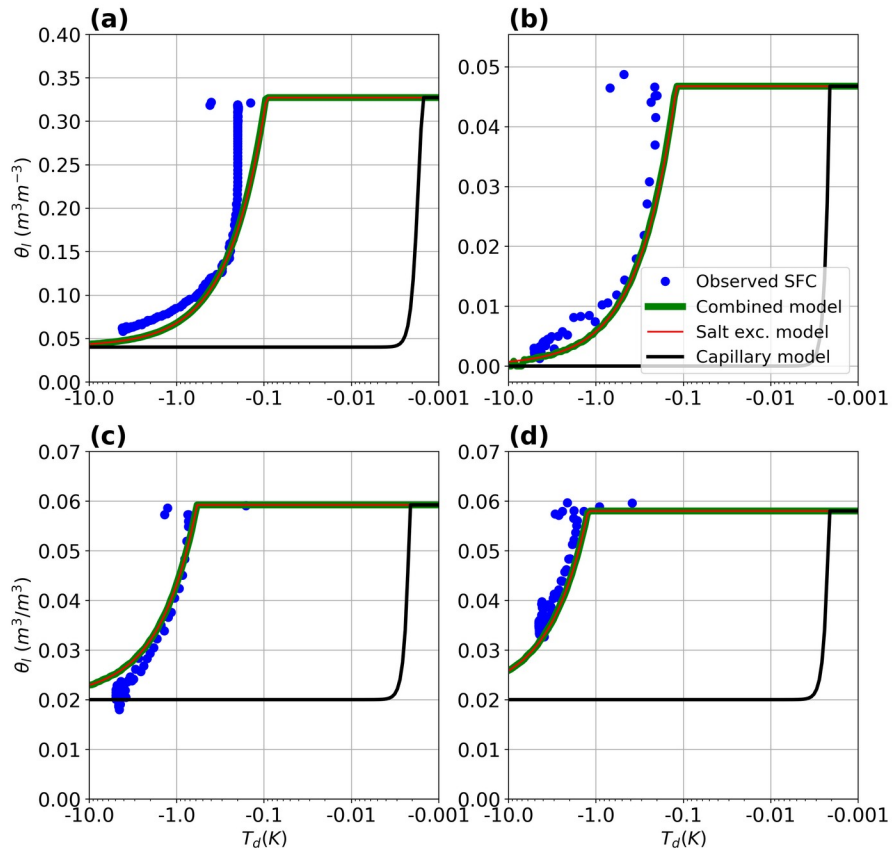
Figure 8. Performance of the three models (capillary, salt-exclusion and combined models) against laboratory observed SFCs at 30 cm depth for different salt concentrations and water contents: (a) $c_b = ¿0.48$ g l^{-1}; high moisture content (b) $c_b = ¿0.1$ g l^{-1} ; low moisture content (c) $c_b = ¿0.4$ g l^{-1} ; low moisture content, and (d) $c_b = ¿ 0.8$ g l^{-1}; low moisture content.

Figure 9 and Figure 10 show the performance of the three models at the SDN and OJP field sites, respectively. The models were first run without salt ($c_b = 0$, Figure 9a and Figure 10a) and then by adding arbitrary amounts of salt to fit the models to the observed SFCs (Figure 9b and 10b). Note that at SDN the largest adjustments to θ_r were made, and it is clear from the observations alone (Figure 5) that there are significant differences in the lower limit of the liquid water content for drying and freezing. The model results show that for both field sites (SDN and OJP), the capillary model and the identical combined model with zero salt underestimated freezing point depression (Figure 9a and 10a). This is less surprising than for the laboratory experiments because we expect significant amounts of dissolved salts in these field soils. The underestimation is smaller at the OJP site (Figure 10a) than at the SDN site (Figure 9a), which was also expected because the OJP site has less saline soil, and thus, the salt exclusion effect

570   should be smaller. Again, the salt exclusion model failed as expected when no salt was added to the model. In Figure

571   9b and 10b salt was added to the model to fit the observed SFCs, and here both the salt exclusion and the combined

572   model did well in predicting the observed SFCs for both field sites (Figure 9b and 10b). Comparing the average salt

573   concentration used in the fitting run for the SDN site to those used at the OJP site (Table 7), we see that the SDN site

574   has more salt than the OJP site, which is correct.
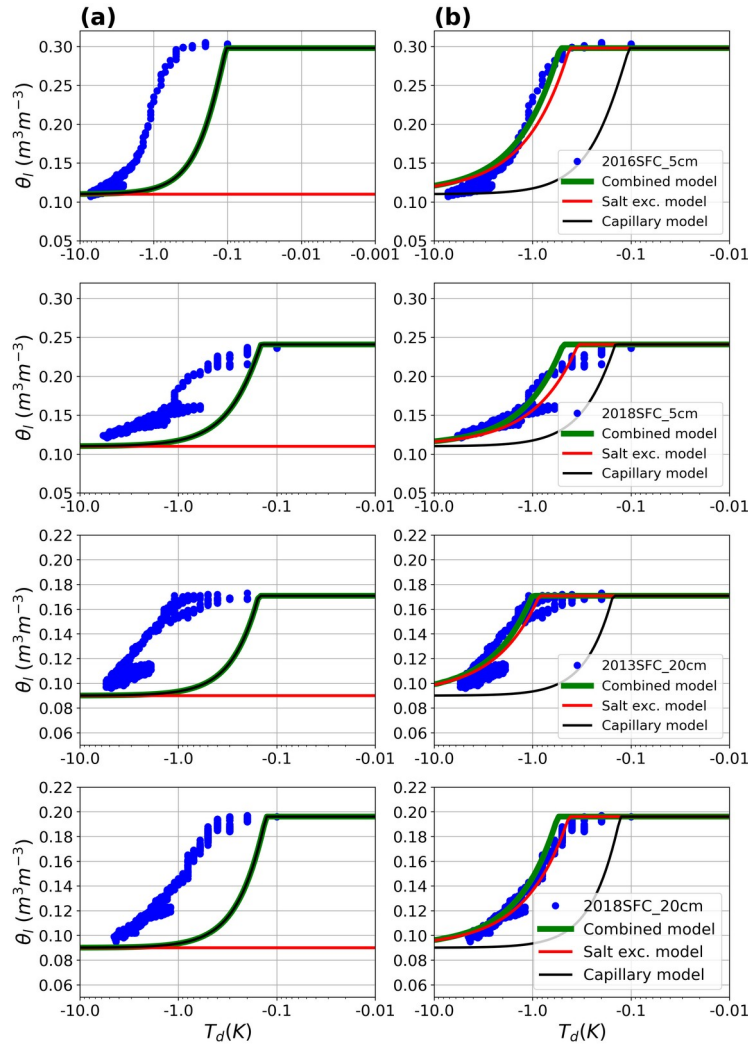
575

576   **Figure 9**. Performance of the three models (capillary, salt-exclusion and combined capillary salt model) against

577   observed SFCs for SDN site; a) models applied without salt and, b) model fitted to the observed SFCs by adjusting

578   the salt masses.
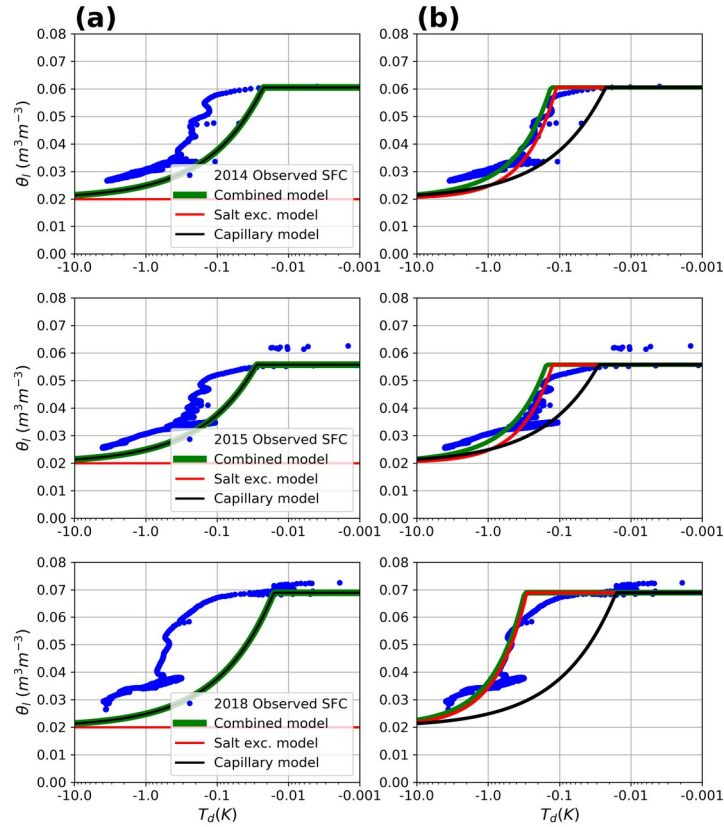
579

580   **Figure 10**. Performance of the three models (capillary, salt-exclusion and combined capillary salt model) against

581   observed SFCs for OJP site ; a) models applied without salt and, b) model fitted to the observed SFCs by adjusting

582   the salt masses.

583

584   **Table 7**

585   *Bulk salt Concentration (c_b) used in the fitting runs for the SDN and OJP field sites*

SDN site		OJP site	
Year and depth	c_b (g l^{-1})	Year	c_b (g l^{-1})
2016 5cm	1.4	2014	0.08
2018 5cm	0.8	2015	0.08
2013 20cm	1.2	2018	0.25
2018 20 cm	0.8	-	-
Average	1.05	Average	0.14

586   **4 Conclusions**

587   In this study, SMCs and SFCs were measured for soils with varying texture and salinity in laboratory and field

588   conditions, using dielectric impedance probes to measure the liquid water content. In our seasonally frozen field

589   sites, SFCs have a number of important characteristics, which we summarize conceptually in Figure 11, and describe

590   here: *i)* the antecedent water content prior to freezing are normally not saturated, and may in fact be quite dry,

591   meaning that assuming saturated soils for frozen conditions is likely to introduce significant errors; *ii)* the freezing

592   and thawing curves are distinctly hysteretic (consistent with previously reported curves from Koopmans and Miller,

593   1966, Tice et al., 1989, and Watanabe and Osada, 2017); and *iii)* the soils are wetter, and perhaps saturated, at the

594   end of thawing, which is due to a combination of possible soil moisture redistribution by cryosuction during the

595   winter, and snowmelt infiltration during the melt period.

596
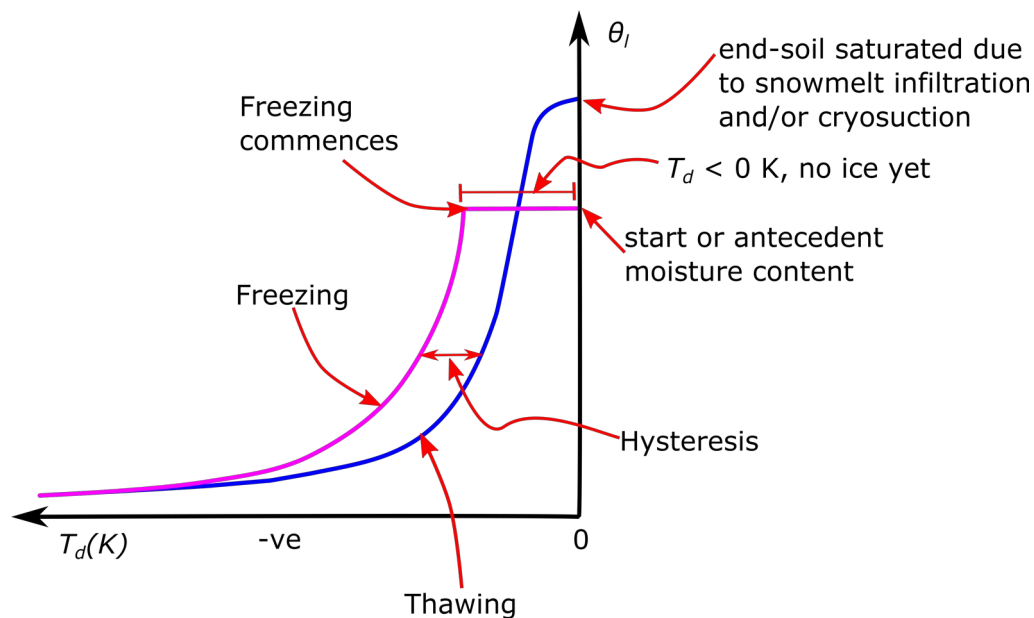
597

598   **Figure 11**: Conceptual diagram depicting the difference between freezing and thawing in frozen soils

599   Three alternative models were developed to simulate the SFC: a capillary model, based on the GCE; a salt exclusion

600   model; and a combined model. The combined model is identical to the capillary model when there is no salt in the

601   soil, and identical to the salt exclusion model when salt concentrations are high. The salt exclusion model fails to

602   predict any freezing point depression when there is no salt in the pore water (though such completely salt-free

603   conditions do not exist in real soils anywhere). In the salt exclusion and combined model, the effect of adding more

604   salt is to increase the amount of freezing point depression progressively.

605 The three alternative models were tested against our observed SFCs. In all cases, we found that the capillary model
606 (GCE) significantly under-predicted freezing point depression (that is, the temperature for a given liquid water
607 content is under-predicted, or equivalently, the liquid water content for a given temperature is under-predicted). In
608 the controlled salinity lab experiments, we found excellent agreement between the salt exclusion and combined
609 models, with no fitting (i.e. calibration). However, for the zero salinity case, the models all failed, unless we
610 introduced a small amount of salt. By fitting the model in this way the salt exclusion and combined models
611 performed well. We also found that to define the SFC it was necessary to reduce the residual water content from that
612 used in the SMC, and we speculate that this is a real phenomenon, where ice is able to propagate into smaller pores
613 during freezing than air is during drying.

614 Our results suggest that, at least for the soils we considered, salt exclusion effects on freezing point depression are
615 more important than capillary effects. The widely used GCE is likely to under-predict freezing point depression. The
616 consequence of this is that for a given subzero temperature, the equivalent matric potential caused by freezing, as
617 predicted by the GCE, is too low, which in coupled models is likely to lead to significant over estimates of hydraulic
618 gradients associated with cryosuction, and associated numerical instabilities. It would be valuable in future work to
619 explore the consequences of the salt-exclusion model in coupled models.

Acknowledgments, Samples, and Data

628 On acceptance of the paper, all field and lab data used will be uploaded to the Canadian Federated Research Data
629 Repository at: https://www.frdr-dfdr.ca/repo/ and assigned a DOI number. In the meantime, the data are included in
630 the supplementary material.

References

632 Azmatch, T. F., Sego, D. C., Arenson, L. U., & Biggar, K. W. (2012). Using soil freezing characteristic curve to
633 estimate the hydraulic conductivity function of partially frozen soils. *Cold Regions Science and Technology*, *83–84*,
634 103–109. https://doi.org/10.1016/j.coldregions.2012.07.002

635 Bam, E. K. P., Brannen, R., Budhathoki, S., Ireson, A. M., & Spence, C. (2019). Meteorological, soil moisture,
636 surface water, and groundwater data from the St. Denis National Wildlife Area, Saskatchewan, Canada. 11. *Earth*
637 *System Science Data Discussions* (pp 1-21). https://doi.org/10.5194/essd-2018-125

638 Bam, E. K. P., & Ireson, A. M. (2019). Quantifying the wetland water balance: A new isotope-based approach that
639 includes precipitation and infiltration. *Journal of Hydrology*, *570*, 185–200.
640 https://doi.org/10.1016/j.jhydrol.2018.12.032

641   Banin, A., & Anderson, D. M. (1974). Effects of salt concentration changes during freezing on the unfrozen water
642   Content of porous materials. *Water Resources Research*, *10*(1), 124–128.
643   https://doi.org/10.1029/WR010i001p00124

644   Barr, A. G., van der Kamp, G., Black, T. A., McCaughey, J. H., & Nesic, Z. (2012). Energy balance closure at the
645   BERMS flux towers in relation to the water balance of the White Gull Creek watershed 1999–2009. *Agricultural*
646   *and Forest Meteorology*, *153*, 3–13.

647   Bitelli, M., Flury, M., & Campbell, G. S. (2003). A thermodielectric analyzer to measure the freezing and moisture
648   characteristic of porous media. *Water Resources Research*, *39*(2). https://doi.org/10.1029/2001WR000930

649   Budhathoki, S. (2018). Modelling snowmelt infiltration processes in seasonally frozen ground [Thesis, University of
650   Saskatchewan]. https://harvest.usask.ca/handle/10388/8468

651   Caicedo, B. (2017). Physical modelling of freezing and thawing of unsaturated soils. *Géotechnique*, *67*(2), 106–126.
652   https://doi.org/10.1680/jgeot.15.P.098

653   Chang, C., Sommerfeldt, T. G., Carefoot, J. M., & Schaalje, G. B. (1983). Relationships of electrical conductivity
654   with total dissolved salts and cation concentration of sulfate-dominant soil extracts. *Canadian Journal of Soil*
655   *Science*, *63*(1), 79–86. https://doi.org/10.4141/cjss83-008
656

657   Christensen, A. F., He, H., Dyck, M. F., Lenore Turner, E., Chanasyk, D. S., Naeth, M. A., & Nichol, C. (2013). In
658   situ measurement of snowmelt infiltration under various topsoil cap thicknesses on a reclaimed site. *Canadian*
659   *Journal of Soil Science*, *93*(4), 497–510. https://doi.org/10.4141/cjss2012-048

660   Clark, M. P., Nijssen, B., Lundquist, J. D., Kavetski, D., Rupp, D. E., Woods, R. A., Freer, J. E., Gutmann, E. D.,
661   Wood, A. W., Gochis, D. J., Rasmussen, R. M., Tarboton, D. G., Mahat, V., Flerchinger, G. N., & Marks, D. G.
662   (2015). A unified approach for process-based hydrologic modeling: 2. Model implementation and case studies.
663   *Water Resources Research*, 51(4), 2515–2542. https://doi.org/10.1002/2015WR017200

664   Cuenca, R. H., Stangel, D. E., & Kelly, S. F. (1997). Soil water balance in a boreal forest. *Journal of Geophysical*
665   *Research: Atmospheres*, *102*(D24), 29355–29365. https://doi.org/10.1029/97JD02312

666   Dall'Amico, M., Endrizzi, S., Gruber, S., & Rigon, R. (2011). A robust and energy-conserving model of freezing
667   variably saturated soil. *The Cryosphere*, *5*(2), 469–484. https://doi.org/10.5194/tc-5-469-2011

668   Flerchinger, G. N., Seyfried, M. S., & Hardegree, S. P. (2006). Using soil freezing characteristics to model multi-
669   season soil water dynamics. *Vadose Zone Journal*, *5*(4), 1143. https://doi.org/10.2136/vzj2006.0025

670   Francisca, F. M., & Montoro, M. A. (2012). Measuring the dielectric properties of soil–organic mixtures using
671   coaxial impedance dielectric reflectometry. *Journal of Applied Geophysics*, *80*, 101–109.
672   https://doi.org/10.1016/j.jappgeo.2012.01.011

673   Gray, D. M., & Granger, R. J. (1986). In situ measurements of moisture and salt movement in freezing soils.
674   *Canadian Journal of Earth Sciences*, *23*(5), 696–704. https://doi.org/10.1139/e86-069

675   Gharedaghloo, B., Berg, S. J., & Sudicky, E. A. (2020). Water freezing characteristics in granular soils: Insights
676   from pore-scale simulations. *Advances in Water Resources*, *143*, 103681.
677   https://doi.org/10.1016/j.advwatres.2020.103681

678   Haghighi, H., Chapoy, A., & Tohidi, B. (2008). Freezing point depression of electrolyte solutions: Experimental
679   measurements and modeling using the cubic-plus-association equation of state. *Industrial & Engineering Chemistry*
680   *Research*, *47*(11), 3983–3989. https://doi.org/10.1021/ie800017e

681   Hayashi, M. (2013). The cold vadose zone: Hydrological and ecological significance of frozen-soil processes.
682   *Vadose Zone Journal*, *12*(4), 1-8.

683   Hayashi, M., van der Kamp, G., & Rudolph, D. L. (1998). Water and solute transfer between a prairie wetland and
684   adjacent uplands, 2. Chloride cycle. *Journal of Hydrology*, *207*(1–2), 56–67. https://doi.org/10.1016/S0022-
685   1694(98)00099-7

686 He, H., Dyck, M., Zhao, Y., Si, B., Jin, H., Zhang, T., Lv, J., & Wang, J. (2016). Evaluation of five composite
687 dielectric mixing models for understanding relationships between effective permittivity and unfrozen water content.
688 *Cold Regions Science and Technology*, *130*, 33–42.

689 Hansson, K., Šimůnek, J., Mizoguchi, M., Lundin, L.-C., & Genuchten, M. T. van. (2004). Water flow and heat
690 transport in frozen soil: Numerical solution and freeze–thaw applications. *Vadose Zone Journal*, *3*(2), 693–704.
691 https://doi.org/10.2136/vzj2004.0693

692 Ireson, A. M., Barr, A. G., Johnstone, J. F., Mamet, S. D., Van Der Kamp, G., Whitfield, C. J., Michel, N. L., North,
693 R. L., Westbrook, C. J., Debeer, C., Chun, K. P., Nazemi, A., & Sagin, J. (2015). The changing water cycle: The
694 boreal plains ecozone of Western Canada. *Wiley Interdisciplinary Reviews: Water*, *2*(5), 505–521.
695 https://doi.org/10.1002/wat2.1098

696 Kelleners, T. J., Paige, G. B., & Gray, S. T. (2009). Measurement of the Dielectric Properties of Wyoming Soils
697 Using Electromagnetic Sensors. *Soil Science Society of America Journal*, *73*(5), 1626.
698 https://doi.org/10.2136/sssaj2008.0361

699 Kelleners, T. J., & Verma, A. K. (2010). Measured and Modeled Dielectric Properties of Soils at 50 Megahertz. *Soil
700 Science Society of America Journal*, *74*(3), 744–752. https://doi.org/10.2136/sssaj2009.0359

701 Kelleners, T. J., & Norton, J. B. (2012). Determining water retention in seasonally frozen soils using hydra
702 impedance sensors. *Soil Science Society of America Journal*, *76*(1), 36. https://doi.org/10.2136/sssaj2011.0222

703 Koopmans, R. W. R., & Miller, R. D. (1966). Soil freezing and soil water characteristic curves. *Soil Science Society
704 of America Journal*, *30*(6), 680–685.

705 Kozlowski, T. (2009). Some factors affecting supercooling and the equilibrium freezing point in soil–water systems.
706 *Cold Regions Science and Technology*, *59*(1), 25–33. https://doi.org/10.1016/j.coldregions.2009.05.009

707 Kurylyk, B. L., & Watanabe, K. (2013). The mathematical representation of freezing and thawing processes in
708 variably saturated, non-deformable soils. *Advances in Water Resources*, *60*, 160–177.
709 https://doi.org/10.1016/j.advwatres.2013.07.016

710 Mizoguchi, M. (1990). Water, heat and salt transport in freezing soil [PhD thesis In Japanese, University of Tokyo,
711 Japan].

712 Mohammed, A. A., Kurylyk, B. L., Cey, E. E., & Hayashi, M. (2018). Snowmelt Infiltration and macropore flow in
713 frozen soils: Overview, knowledge gaps, and a conceptual framework. *Vadose Zone Journal*, *17*(1).
714 https://doi.org/10.2136/vzj2018.04.0084

715 Nachshon, U., Ireson, A., van der Kamp, G., Davies, S. R., & Wheater, H. S. (2014). Impacts of climate variability
716 on wetland salinization in the North American prairies. *Hydrology and Earth System Sciences*, *18*(4), 1251–1263.
717 https://doi.org/10.5194/hess-18-1251-2014

718 Nazarbakhsh, M., Ireson, A. M., & Barr, A. G. (2020). Controls on evapotranspiration from jack pine forests in the
719 Boreal Plains Ecozone. *Hydrological Processes*, *34*(4), 927–940. https://doi.org/10.1002/hyp.13674

720 Oquist, M. G., Sparrman, T., Klemedtsson, L., Drotz, S. H., Grip, H., Schleucher, J., & Nilsson, M. (2009). Water
721 availability controls microbial temperature responses in frozen soil CO_2 production. *Global Change Biology*,
722 *15*(11), 2715–2722. https://doi.org/10.1111/j.1365-2486.2009.01898.x

723 Painter, S. L., & Karra, S. (2014). Constitutive Model for Unfrozen Water Content in Subfreezing Unsaturated Soils.
724 Vadose Zone Journal, 13(4), vzj2013.04.0071. https://doi.org/10.2136/vzj2013.04.0071

725 Patterson, D. E., & Smith, M. W. (1985). Unfrozen water content in saline soils: results using time-domain
726 reflectometry. *Canadian Geotechnical Journal*, *22*(1), 95–101.

727 Pekrioglu Balkis, A. (2019). Determination of SWRC for unsaturated sands, comparative study – Filter paper
728 method versus hanging column technique. *European Journal of Science and Technology*, (16), 403–413.
729 https://doi.org/10.31590/ejosat.539620

730 Pires, L. F., Brinatti, A. M., & Saab, S. da C. (2015). Experimental method to determine some physical properties in
731 physics classes. *Revista Brasileira de Ciência Do Solo*, *39*(5), 1507–1512.
732 https://doi.org/10.1590/01000683rbcs20140766

733 Ren, J., & Vanapalli, S. K. (2019). Comparison of Soil-Freezing and Soil-Water Characteristic Curves of Two
734 Canadian Soils. *Vadose Zone Journal*, *18*(1). https://doi.org/10.2136/vzj2018.10.0185
735

736 Ren, J., & Vanapalli, S. K. (2020). Effect of freeze–thaw cycling on the soil-freezing characteristic curve of five
737 Canadian soils. *Vadose Zone Journal*, *19*(1), e20039. https://doi.org/10.1002/vzj2.20039

738 Rohatgi, A. (2015). *WebPlotDigitizer User Manual Version 3.9*. 23.

739 Schafer, H. L., & Beier, N. A. (2017). Development of soil freezing characteristic curves for fluid fine tailings using
740 TDR. *Geo Ottawa 2017*.

741 Schofield, R. K. (1935). The pF of the water in soil. *Third International Congress of Soil Science*, *2*, 37–48.

742 Seyfried, M. S., & Murdock, M. D. (2004). Measurement of soil water content with a 50-MHz soil dielectric sensor.
743 *Soil Science Society of America Journal*, *68*(2), 394–403. https://doi.org/10.2136/sssaj2004.3940

744 Spaans, E. J. A. (1994). The soil freezing characteristic: Its measurement and similarity to the soil moisture
745 characteristic [PhD thesis]. University of Michigan.
746

747 Spaans, E. J. A., & Baker, J. M. (1995). Examining the use of time domain reflectometry for measuring liquid water
748 content in frozen soil. *Water Resources Research*, *31*(12), 2917–2925. https://doi.org/10.1029/95WR02769

749 Spaans, E. J. A., & Baker, J. M. (1996). The soil freezing characteristic: Its measurement and similarity to the soil
750 moisture characteristic. *Soil Sci. Soc. Am. J.*, *60*, 13–19.

751 Stähli, M., & Stadler, D. (1997). Measurement of water and solute dynamics in freezing soil columns with time
752 domain reflectometry. *Journal of Hydrology*, *195*(1), 352–369. https://doi.org/10.1016/S0022-1694(96)03227-1
753

754 Stevens Water Monitoring Systems Inc.: The Hydra Probe® Soil Sensor, User's Manual, 1–63, July 2007.

755 Susha Lekshmi, S. U., Singh, D. N., & Shojaei Baghini, M. (2014). A critical review of soil moisture measurement.
756 *Measurement*, *54*, 92–105. https://doi.org/10.1016/j.measurement.2014.04.007

757 Teng, J. (2020). Parameterization of soil freezing characteristic curve for unsaturated soils. *Cold Regions Science*
758 *and Technology*, 8.

759 Tian, Z., Ren, T., Kojima, Y., Lu, Y., Horton, R., & Heitman, J. L. (2017). An improved thermo-time domain
760 reflectometry method for determination of ice contents in partially frozen soils. *Journal of Hydrology*, *555*, 786–
761 796. https://doi.org/10.1016/j.jhydrol.2017.10.055

762 Tian, H., Wei, C., Lai, Y., & Chen, P. (2018). Quantification of Water Content during Freeze–Thaw Cycles: A
763 Nuclear Magnetic Resonance Based Method. *Vadose Zone Journal*, *17*(1), 160124.
764 https://doi.org/10.2136/vzj2016.12.0124
765

766 Tice, A. R., Black, P. B., & Berg, R. L. (1989). Unfrozen water contents of undisturbed and remolded Alaskan silt.
767 *Cold Regions Science and Technology*, *17*(2), 103–111. https://doi.org/10.1016/S0165-232X(89)80001-1

768 Tice, A. R., Oliphant, J., Nakano, Y., & Jenkins, T. F. (1982). Relationship between the Ice and Unfrozen Water
769 Phases in Frozen Soil as Determined by Pulsed Nuclear Magnetic Resonance and Physical Desorption Data. US
770 Army Corps of Engineers, CRREL Report 82-15.

771 UMS (2015): Manual HYPROP, version 2015-01, 99 pp. UMS GmbH, Gmunder Strabe 37 Munich, Germany.
772 http://ums-muc.de/static/Manual_HYPROP.pd

773 van Genuchten, M. (1980). A closed-form equation for predicting the hydraulic conductivity of unsaturated soils 1.
774 *Soil Science Society of America Journal*, *44*(5), 892–898.
775 https://doi.org/10.2136/sssaj1980.03615995004400050002x

776 Watanabe, K., Kito, T., Wake, T., & Sakai, M. (2011). Freezing experiments on unsaturated sand, loam and silt
777 loam. *Annals of Glaciology*, *52*(58), 37–43. https://doi.org/10.3189/172756411797252220

778 Watanabe, K., & Mizoguchi, M. (2002). Amount of unfrozen water in frozen porous media saturated with solution.
779 *Cold Regions Science and Technology*, *34*(2), 103–110. https://doi.org/10.1016/S0165-232X(01)00063-5

Watanabe, K., & Osada, Y. (2017). Simultaneous measurement of unfrozen water content and hydraulic conductivity of partially frozen soil near 0 °C. *Cold Regions Science and Technology*, *142*, 79–84. https://doi.org/10.1016/j.coldregions.2017.08.002

Watanabe, K., & Wake, T. (2009). Measurement of unfrozen water content and relative permittivity of frozen unsaturated soil using NMR and TDR. *Cold Regions Science and Technology*, *59*(1), 34–41. https://doi.org/10.1016/j.coldregions.2009.05.011

Wen, Z., Ma, W., Feng, W., Deng, Y., Wang, D., Fan, Z., & Zhou, C. (2012). Experimental study on unfrozen water content and soil matric potential of Qinghai-Tibetan silty clay. *Environmental Earth Sciences*, *66*(5), 1467–1476. https://doi.org/10.1007/s12665-011-1386-0

Williams, P. J., & Smith, M. W. (1989). The frozen earth. Cambridge University Press.

Williams, P. J. (1970). Properties and behaviour of freezing soils. *Norwegian Geotechnical Institute*, *72*.

Williams, P. J. (1964). Unfrozen water content of frozen soils and soil moisture suction. *Géotechnique*, *14*(3), 231–246. https://doi.org/10.1680/geot.1964.14.3.231

Yan, G., Li, Z., Bore, T., Scheuermann, A., Galindo-Torres, S., & Li, L. (2017). The measurement of primary drainage curve using hanging column and large soil column test. ResearchGate. https://www.researchgate.net/publication/318734619

Yao, Y.-S., Zheng, J.-L., Chen, Z.-S., Zhang, J.-H., & Li, Y. (2016). Field measurements and numerical simulations of temperature and moisture in highway engineering using a frequency domain reflectometry sensor. *Sensors (Basel, Switzerland)*, *16*(6). https://doi.org/10.3390/s16060857

Yoshikawa, K., & Overduin, P. P. (2005). Comparing unfrozen water content measurements of frozen soil using recently developed commercial sensors. *Cold Regions Science and Technology*, *42*(3), 250–256. https://doi.org/10.1016/j.coldregions.2005.03.001

Zhang, C., & Liu, Z. (2018). Freezing of water confined in porous materials: role of adsorption and unfreezable threshold. *Acta Geotechnica*, *13*(5), 1203–1213. https://doi.org/10.1007/s11440-018-0637-6

Zhou, J., Wei, C., Lai, Y., Wei, H., & Tian, H. (2018). Application of the generalized clapeyron equation to freezing point depression and unfrozen water content. *Water Resources Research*, *54*(11), 9412–9431. https://doi.org/10.1029/2018WR023221

Zhou, J., Meng, X., Wei, C., & Pei, W. (2020). Unified soil freezing characteristic for variably-saturated saline soils. *Water Resources Research*, *56*(7), e2019WR026648. https://doi.org/10.1029/2019WR026648

Zhou, X., Zhou, J., Kinzelbach, W., & Stauffer, F. (2014). Simultaneous measurement of unfrozen water content and ice content in frozen soil using gamma ray attenuation and TDR. *Water Resources Research*, *50*(12), 9630–9655. https://doi.org/10.1002/2014WR015